Dynamic holography for optical interconnections. II. Routing holograms with predictable location and intensity of each diffraction order

Kim L. Tan*

Department of Engineering, Cambridge University, Trumpington Street, Cambridge CB2 1PZ, UK

Stephen T. Warr

Thomas Swan & Co. Ltd., c/o Department of Engineering, Cambridge University, Trumpington Street, Cambridge CB2 1PZ, UK

Ilias G. Manolis, Timothy D. Wilkinson, Maura M. Redmond, William A. Crossland, and Robert J. Mears

Department of Engineering, Cambridge University, Trumpington Street, Cambridge CB2 1PZ, UK

Brian Robertson

Thomas Swan & Co., Ltd. c/o Department of Engineering, Cambridge University, Trumpington Street, Cambridge CB2 1PZ, UK

Received October 19, 1999; revised manuscript received June 20, 2000; accepted July 25, 2000

An analysis of dynamic phase-only holograms, described by fractional notation and recorded onto a pixelated spatial light modulator (SLM) in a reconfigurable optical beam-steering switch, is presented. The phase quantization and arrangement of the phase states and the SLM pixelation and dead-space effects are decoupled, expressed analytically, and simulated numerically. The phase analysis with a skip–rotate rule reveals the location and intensity of each diffraction order at the digital replay stage. The optical reconstruction of the holograms recorded onto SLM's with rectangular pixel apertures entails sinc-squared scaling, which further reduces the intensity of each diffraction order. With these two factors taken into account, the highest values of the nonuniform first-order diffraction efficiencies are expected to be 33%, 66%, and 77% for two-, four-, and and eight-level one-dimensional holograms with a 90% linear pixel fill factor. The variation of the first-order diffraction efficiency and the relative replay intensities were verified to within 1 dB by performing the optical reconstruction of binary phase-only holograms recorded onto a ferroelectric liquid crystal on a silicon SLM. © 2001 Optical Society of America

OCIS codes: 050.1950, 090.1760, 090.2890, 100.5090, 120.5060, 230.6120.

1. INTRODUCTION

In Part I,[1] the effects of hologram illumination on the replay beam profile, the on-beam-axis coupling efficiency, and the cross-talk isolation of a 4*f* holographic switch were presented. For dynamic holographic routing with a reconfigurable spatial light modulator (SLM), the conventional grating description in terms of its physical pitch length and analysis as a step-phase function[2] are both cumbersome and inadequate: cumbersome because the physical parameters of a holographic replay are not necessarily required or known when one is analyzing a holographic switch and inadequate because gratings (see Subsection 2.A) form only a subset of all possible routing patterns with a pixelated SLM with inherent physical limitations. Another way to replay arbitrary hologram functions encoded onto SLM's with pixel defects is to perform a discrete Fourier transform (DFT; e.g., a fast-Fourier-transform algorithm[3]) on the zero-padded, oversampled digital representation of the optical holograms. Clearly, the computing resources required for the DFT and for evaluating the efficiency of the main replay order and the potential cross talk of each noise order can be prohibitive for large hologram array sizes.

Hence, here we treat the phase and the spatial effects that determine the intensity and location of each far-field, Fraunhofer diffraction order or peak (henceforth called replay order) separately in analytic forms. For the analyses we utilize the fractional hologram representation described in Subsection 2.A. In the context of optical reconstruction of thin holograms, Subsection 2.B illustrates the typically convoluted phase and spatial effects.

The phase effect is concerned with quantization with a limited number of phase levels and the dynamic hologram patterns (i.e., the distribution of phase elements) within each hologram unit (or base hologram) at the digital synthesis–reconstruction stage. An equation that describes the intensity of all the replay orders in an aliased digital replay (i.e., which comprises Dirac delta functions)

DOCKET ALARM Find authenticated court documents without watermarks at docketalarm.com.

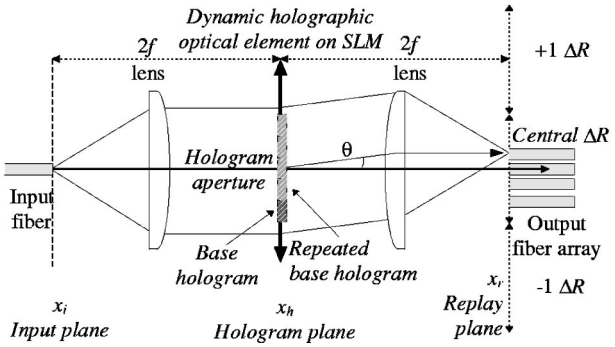

Fig. 1. Free-space $1 \times N$ optical switch with a coherent $4f$ setup. The size of each replay replication, ΔR, is $f\lambda/d$, a consequence of pixel periodicity.

is presented in Subsection 3.B. The locations of these replay orders are to be found by use of a skip–rotate rule such that the intensity expression is applicable. These intensities are exactly as given by a DFT of the hologram.

Recording the optical holograms on a dynamically reconfigurable SLM entails a further drop in replay intensity as a result of pixelation and dead space as well as phase errors (henceforth called the spatial effect). Throughout this analysis, the paraxial optical reconstruction region (an area close to the optical axis at the replay plane where scalar diffraction theory is valid) is divided into subsections of size $f\lambda/d$ centered at the optical axis, where f is the focal length of the transform lens, λ is the wavelength of illumination, and d is the pixel pitch, as shown by the free-space holographic replay system in Fig. 1. These subsections of equal sizes are a result of the pixel periodicity of the pixelated SLM and are called replay replications. Within all replay replications, the distribution of replay orders is identical, except that their intensities are scaled by a sinc-squared roll-off that arises from the pixel transmittance function. For the simplest case of a rectangular pixel aperture, the intensity roll-off expression is given in Subsection 4.A. The effects of SLM pixel imperfection were analyzed for grating replay by use of fixed surface-relief diffractive optical elements (DOE's) etched onto fused silica[4] and optical correlation.[5]

In Section 5 experiments using dynamic holograms recorded onto SLM's for fiber-to-fiber interconnects are described. The results for the relative replay intensities of a particular hologram and the first-order replay efficiencies of several holograms are shown.

2. PROGRAMMABLE DIFFRACTIVE OPTICAL ELEMENTS

Routing holograms are dynamically reconfigurable phase-only holograms that are used in holographic free-space beam steering applications. A single spot replay from either noise- or efficiency-optimized routing holograms is required for one-to-one switch interconnections. An efficiency-optimized computer-generated hologram, obtained by methods such as the inverse DFT, produces only one solution of the phase distribution over a 1-D or two-dimensional (2-D) hologram plane. All phase-shifted or spatially shifted variants of this distribution are eigensets of the original hologram, replaying the same intensity pattern. It is useful to analyze the underlying spatial frequency properties of a general efficiency-optimized hologram as the base case. Noise-optimized holograms, such as those generated by Gerchberg–Saxton,[6] direct binary search,[7] simulated annealing,[8] or error diffusion[9] algorithms, retain the fundamental characteristics of their efficiency-optimized counterparts.

A. Fractional Representation of Routing Holograms

With the DFT analysis and a replay order notation similar to that of Dammann,[2] the numerical intensity replay of an m quantized phase-level, $N \times N$ grid-size hologram is a series of Dirac delta functions:

$$|\hat{h}(x_d, y_d)|^2 = \sum_n \sum_{s\to-\infty}^{\to\infty} \sum_{t\to-\infty}^{\to\infty} \eta_{m;n}^{\xi,\zeta} \delta[x_d - (\langle n\xi + sN\rangle), y_d - (\langle n\zeta + tN\rangle)], \quad (1)$$

where $n = gm + 1$, g being an integer, is the order of replay; (x_d, y_d) is the discrete coordinate at the simulated replay plane; (ξ, ζ) is the coordinate of the first replay order; and $\eta_{m;n}^{\xi,\zeta}$ is the simulated intensity of the nth replay order, given that the hologram encoding is limited to m phase levels. This expression follows directly from the property of the DFT whereby an N-point function is transformed into an N-point replay. Depending on the hologram pattern, one or more numerical replay coordinates will have nonzero intensity. These coordinates are given by modulo-N functions, $\langle n\xi + sN\rangle$ and $\langle n\zeta + tN\rangle$, such that

$$-N/2 \leqslant (\langle n\xi + sN\rangle, \langle n\zeta + tN\rangle) < (N/2), \quad (2)$$

where n and (s, t) can take any values as long as the elements of the set $(\langle n\xi + sN\rangle, \langle n\zeta + tN\rangle)$ are distinct. If (σ, τ) are now assigned as the normalized spatial frequency coordinates (henceforth called fractional coordinates) of the first replay order, (i.e., $\sigma = \xi/N$, $\tau = \zeta/N$), criterion (2) becomes

$$-\tfrac{1}{2} \leqslant (\langle n\sigma + s\rangle, \langle n\tau + t\rangle) < \tfrac{1}{2}, \quad (3)$$

where $\langle n\sigma + s\rangle$ and $\langle n\tau + t\rangle$ are modulo-1 functions. The normalized coordinate of the first replay order is then rewritten as the simplest fraction between two rational numbers, i.e., $\sigma = x/x_0$ and $\tau = y/y_0$, where x and y are integers and x_0 and y_0 are positive integers. All four integers can be odd or even, as is m; and the denominators x_0 and y_0 may or may not be multiples of m. The grating is a special case for which the first-order replay fraction is $(1/x_0, 1/y_0)$ for two dimensions [either $(1/x_0, 0)$ or $(0, 1/y_0)$ for 1-D routing], x_0 and y_0 are multiples of m, and Dammann's efficiency expression [i.e., $\sin^2(n\pi/m)/(n\pi/m)^2$; Ref. 2] is applicable only for the 1-D cases without dead space. The (σ, τ) base hologram requires only four integers for a complete representation of its form by $x_0 \times y_0$ sample points, its replay orders, and the intensities that characterize it. If the $x_0 \times y_0$ size base hologram is repeated on an SLM (with a high-pixel-count $N \times N$ array), generally in any noninteger multiples the number of addressable points is huge ($\gg N^2$).[10] Provided that there is adequate apodization (such as Gaussian) in the illumination, the optical replay of this hologram yields the first diffraction

DOCKET ALARM Find authenticated court documents without watermarks at docketalarm.com.

order at ($\sigma f\lambda/d$, $\tau f\lambda/d$) spatial frequency coordinates from the optical axis. Hence the fractional hologram representation eliminates the need to know the physical parameters of the holographic replay system without compromising any aspect of the hologram properties.

B. Thin Holographic Elements

A general overview of thin holographic elements for steering an incoming beam to a single main order in the paraxial domain (i.e., when the incident angle and the diffraction angle are both small and the transverse feature of the diffractive element is much larger than the illumination wavelength) is shown in Fig. 2. Both the microprism and the step-phase triangular gratings in Figs. 2(a) and 2(b) have the same physical pitch lengths ($8d$, where d is the feature size of the quantized phase steps). They steer the illumination to the desired fractional coordinate (1/8, 2/8, and 3/8 are shown) as a function of the phase depth of the unit element (2π, 4π, and 6π are shown). The difference is that in the latter case there are higher-order replications at multiple integers along the fractional coordinate (lighter arrows) as a result of phase quantization and spatial pixelation of the continuous phase-retardation profile in the former. Blazing the triangular phase profile for a higher order produces an arbitrary steering function by exciting the required replay order (i.e., the main order diffracted to any of the x_0 locations for using x_0 pixels per period). However, this presents severe difficulties in making surface-normal optical components with such considerable depths and numbers of discrete phase steps, and the long optical paths ultimately cause the grating function to depend on the polarization along and orthogonal to the grating line. One useful configuration of the step-phase grating blazed for a higher order is arrayed-waveguide gratings, for which the optical paths are laid out on a planar substrate and hence the path-length difference can be made several tens or hundreds of the center wavelength to disperse a broadband light to several locations.[11]

In making surface-normal optical components one can exploit the modulo-2π property of the phase-retardation profile to wrap any quantized phase level beyond 2π back to the $\{0, 2\pi\}$ range. Figure 2(c) shows the phase profiles of $\sigma = 1/8, 2/8, 3/8$ as well as their corresponding replay images. In most fabrication and encoding techniques for recording fixed DOE's and programmable holograms on SLM's, only a limited number of quantized phase levels m are available ($m \ll x_0$, e.g., $m = 2$ for symmetric replays and more for asymmetric replays). It is possible that phase quantization is out of sync with spatial pixelation; i.e., stepping from one pixel to the next does not involve a single phase step increase or decrease, as shown in Figs. 2(d) and 2(e). Consequently, there are multiple diffraction orders within the central replications, and similar but scaled replay orders that appear at other replications are a result of sampling the optical field at each pixel.

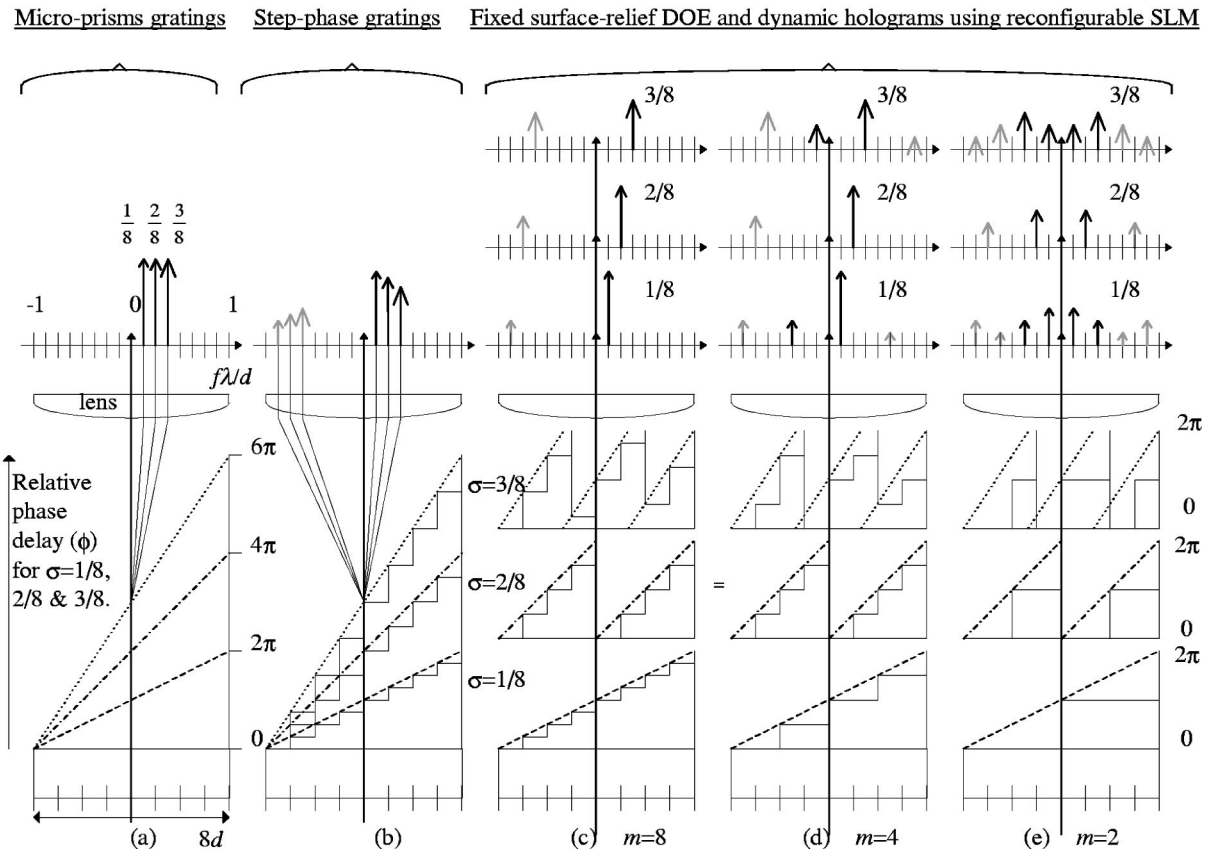

Fig. 2. Beam steering with periodic diffractive optical elements with a full period shown: (a) gratings composed of a microprism array, (b) step-phase gratings blazed for the desired main replay order, (c)–(e) thin optical elements that have only limited numbers of phase levels m, and up to 2π phase depth. With each beam-steering technique the phase profile and the associated replay plane image within the two central replications are depicted for three routing fractions ($\sigma = 1/8, 2/8, 3/8$).

DOCKET ALARM Find authenticated court documents without watermarks at docketalarm.com.

The far-field amplitude of the (n_x, n_y)th diffraction order of a complex-amplitude hologram, H, is often assumed to be[12]

$$h(n_x, n_y) = \left\{ \frac{1}{x_0 y_0} \sum_{k_x=0}^{x_0-1} \sum_{k_y=0}^{y_0-1} H(k_x, k_y) \times \exp\left[2\pi j \left(\frac{n_x k_x}{x_0} + \frac{n_y k_y}{y_0} \right) \right] \right\} \times \{\mathrm{sinc}(\pi n_x / x_0)\mathrm{sinc}(\pi n_y / y_0)\}, \quad (4)$$

where $\mathrm{sinc}(x) = \sin(x)/x$ and the number of pixels in each unit element of the hologram is $x_0 \times y_0$. The phase term, within the normalized double summation [the first set of braces in Eq. (4)], is periodic with respect to x_0 and y_0 and can be evaluated with a DFT algorithm. The double sinc term (in the second set of braces) accounts for the intensity scaling that is due to pixelation without dead space. The orthogonal phase and spatial effects determine the replay intensity and location of each hologram replay order. The replay can be further simplified for routing holograms that steer the light to a single main order.

3. PHASE EFFECT IN DIGITAL REPRESENTATIONS OF ROUTING HOLOGRAMS

In a numerical DFT grating replay in which only a single sampling point for each pixel state is used, an aliased numerical replay will always result, as is consistent with Nyquist's sampling criterion. For example, any integer multiples of a binary $\{0, \pi\}$ phase grating unit will give a replay of 1 unit intensity at the first numerical replay point, corresponding to a $-1/2$ fractional coordinate, as illustrated in Fig. 3(a). Because two sample points are used for each grating period, the highest-frequency component that can be replayed by the DFT is the fundamental frequency. If the fractional coordinate of the first replay order is now $-1/8$ with the use of a binary $\{0\,0\,0\,0\,\pi\,\pi\,\pi\,\pi\}$ phase grating unit, the four times oversampling gives up to four times the fundamental frequency replayed in the same output plane, resulting in four peaks, which appear at ± 1 and ± 3 orders. These two grating functions and their replays as well as those of $\sigma = \pm 1/4$ and $\pm 1/16$ are shown in Fig. 3.

The higher replay orders, exceeding $\pm 1/2$ of a simulated hologram replay grid, should not be thought to be spilling over to the higher replay replications, as each phase element is sampled only by a single point in the numerical DFT and no normalized spatial frequencies of $< -1/2$ or $\geqslant 1/2$ are possible in the numerical replay. Instead, those higher replay orders that overflow the $\pm 1/2$ fractional coordinate at one end must be rolled back into the same numerical replay grid through the opposite end. It is possible that these contributions from infinite higher replay orders overlap exactly the main order or other higher noise orders that are present in the numerical replay grid.

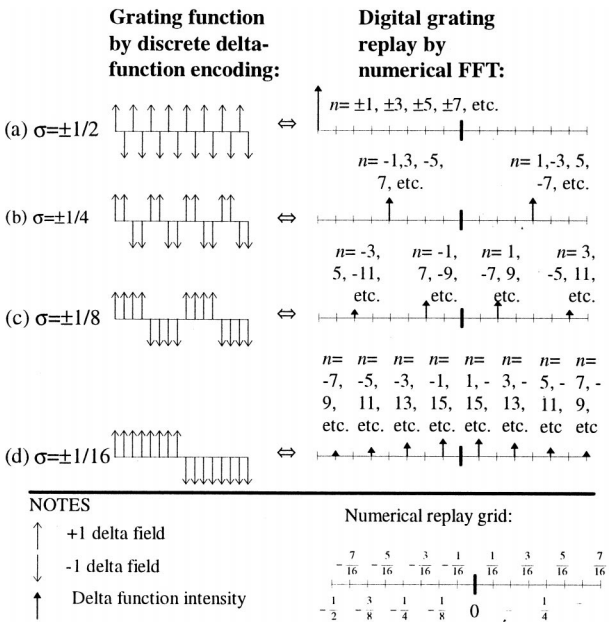

Fig. 3. Overlap of higher replay orders in the numerical replay grid of binary gratings. FFT, fast Fourier transform.

A. Replay Intensities of Grating Holograms

For a general 1-D grating period x_0, the orders that appear within the numerical replay grid as a result of phase quantization and the distribution of x_0 phase elements with m phase states have an aggregated intensity (by summation of the intensities at overlapped positions):

$$\eta_{m;n}^{\sigma} = \sum_{g=-\infty}^{\infty} \mathrm{sinc}^2\left(\frac{n\pi}{m} + g\frac{x_0\pi}{m} \right), \quad (5)$$

where n denotes the replay order and g is an integer. The summation gives the intensity, $\eta_{m;n}^{\sigma}$:

$$\eta_{m;n}^{\sigma} = \mathrm{sinc}^2\left(\frac{n\pi}{m} \right) \sum_{g=-\infty}^{\infty} \left(\frac{n}{n + gx_0} \right)^2. \quad (6)$$

By use of the residue method, the convergent series sums to

$$\eta_{m;n}^{\sigma} = \frac{\mathrm{sinc}^2(n\pi/m)}{\mathrm{sinc}^2(n\pi/x_0)}. \quad (7)$$

Equation (7) gives an accurate description of the intensity of each frequency component that is present in the numerical replay grid. For the $\sigma = \pm 1/2, \pm 1/4, \pm 1/8, \pm 1/16$ binary phase gratings shown in Fig. 3, the first-order intensities are

$$\eta_{m=2;n=\pm 1}^{\sigma=1/2} = \frac{\mathrm{sinc}^2(\pi/2)}{\mathrm{sinc}^2(\pi/2)} = 100\%,$$

$$\eta_{m=2;n=\pm 1}^{\sigma=1/4} = \frac{\mathrm{sinc}^2(\pi/2)}{\mathrm{sinc}^2(\pi/4)} = 50\%,$$

$$\eta_{m=2;n=\pm 1}^{\sigma=1/8} = \frac{\mathrm{sinc}^2(\pi/2)}{\mathrm{sinc}^2(\pi/8)} = 42.68\%,$$

$$\eta_{m=2;n=\pm 1}^{\sigma=1/16} = \frac{\mathrm{sinc}^2(\pi/2)}{\mathrm{sinc}^2(\pi/16)} = 41.05\%, \quad (8)$$

DOCKET ALARM Find authenticated court documents without watermarks at docketalarm.com.

respectively. The number of orders that appear within the N numerical replay points is x_0/m, with a minimum of 1 regardless of m values. As an example, optimization of a four-level phase hologram to route to a $-1/2$ fractional coordinate will always produce a binary grating. Although x_0 is 2 and m is 4 in this case, it should really be considered $m' = 2$, because that is the underlying hologram property for this routing. For a grating that consists of as many encoding elements as there are phase levels (e.g., $\sigma = 1/4$, $m = 4$; $\sigma = 1/5$, $m = 5$, etc.), the grating's numerical replay will always contain a single order of 100%. This means that the phase effect produces 100% efficiency [$x_0 = m$ in Eq. (7)].

In the actual grating encoding that uses rectangular- or square-aperture pixels and optical grating replay by the use of a transform lens, each harmonic frequency component will be revealed with appropriate intensity scaling by the transform of the pixel aperture function. In the ideal situation in which the grating is an infinite repetition of an m-level phase ramp, the pixel aperture is rectangular or square without dead space, and the grating illumination is an infinite-expanse plane wave, the reverse process of the summation in Eq. (5) takes place. The spatial term of a grating effectively cancels out the denominator of Eq. (7) to yield Dammann's expression.[2] Decoupling the phase effect from the overall efficiency expression is important because many arbitrary 2-D hologram patterns in addition to 1-D gratings are often required, the parameters of the intensity scaling term are dependent on the recording device, and the spatial effect in general does not cancel out the denominator of Eq. (7) to yield Dammann's expression of hologram replay efficiency.

B. Replay Intensities of General Holograms

At the digital stage, the numerical replay field of a general 1-D phase-only hologram of a $\sigma = x/x_0$ first-order replay fraction contains the same fundamental properties as the $1/x_0$ phase-only hologram. The relative intensities of all the replay orders that are present are redistributed according to which harmonic of the basic $1/x_0$ hologram is excited. Extending the analysis to general 2-D holograms, we use the least-common multiple of m, x_0, and y_0 [Eq. (7)] to enhance the intensity of each overlapped location within the numerical replay grid:

$$\eta_{m;n}^{\sigma,\tau} = \frac{\operatorname{sinc}^2(n\pi/m)}{\operatorname{sinc}^2[n\pi/lcm(m, x_0, y_0)]}, \tag{9}$$

where $lcm(m, x_0, y_0)$ takes the least common multiple of m, x_0 and y_0, either x_0 or y_0 is assumed 1 for general 1-D holograms, and $m \geq 2$. There are $lcm(m, x_0 y_0)/m$ nonzero intensity orders within $x_0 \times y_0$ points in the numerical replay grid. It is important that 2-D Fourier (continually shifted) phase-only holograms rather than crossed holograms be replayed. The crossed phase-only holograms can be considered to be producing independent routings in the x and y directions, giving many additional orders in the numerical replay grid.

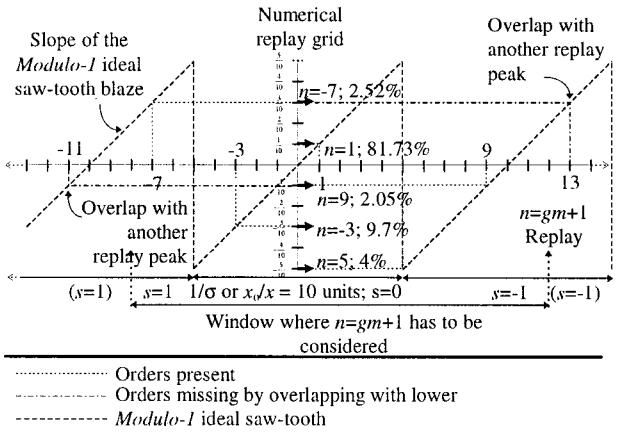

Fig. 4. Modulo-1 skip–rotate rule used to locate higher replay orders of a $\sigma = 1/10$ quaternary hologram replay fraction.

C. Replay Locations of General Holograms

One can predict the location of each replay order by folding higher replay orders with fractional locations of $<-1/2$ or $\geq 1/2$ back to the numerical replay grid. Identifying the location of each order (or equivalently the order number at each nonzero location) enables the intensities to be calculated from Eq. (9). The modulo-1 skip–rotate rule is illustrated in Fig. 4 for a 1-D numerical replay with $\sigma = 1/10$ and $m = 4$. It has been assumed that the phase-matching condition is satisfied (i.e., that there is a $2\pi(m-1)/m$ phase depth between the lowest and the highest phase levels.

The key to obtaining the correct number of n orders that appear in the numerical replay grid is to draw an ideal saw-toothed blaze along the n axis passing through $n = 0$ and the center of the 1-D numerical replay grid with a slope of x and a period of $1/\sigma$. The orders that do appear in the numerical replay grid have decreasing intensities in accordance with Dammann's criterion, $n = gm + 1$, where $g = 0, -1, +1, -2, +2, -3, +3\ldots$. Each integer g is taken successively until a high order begins to overlap one of the existing replay orders (i.e., only the lowest $lcm(m, x_0)/m$ orders at $\pm$ frequencies need to be considered). The overlap of a higher replay order with an existing replay order occurs only after every $lcm(m, x_0)$-order separation, or 20 separations for the hologram shown. We take the example of $n = -7$ order; its replay location (i.e., $n \times \sigma$ or $-7/10$) is folded by the ideal saw-toothed blaze to 3/10 along the unit replay grid. The intensity of this aliased replay peak has contributions from $n = -7, 13, -27, 33, \ldots$. Thus the aggregate intensity is $\operatorname{sinc}^2(-7\pi/4) + \operatorname{sinc}^2(13\pi/4) + \operatorname{sinc}^2(-27\pi/4) + \operatorname{sinc}^2(33\pi/4) + \ldots$, or 2.52%, as given by the infinite sum in Eq. (9) with $y_0 = 1$.

Extending the skip–rotate rule to the replay of 2-D Fourier holograms, we apply the modulo-1 function to both the x and the y directions, resulting in an $(x\mathbf{i} + y\mathbf{i})$ base vector and its multiples folding back to the $\{-1/2, 1/2\}$ unit replay grid from top to bottom and right to left, and vice versa. The locations of the first ten replay orders for a (1/10, 3/8) base hologram are shown in Fig. 5.

DOCKET ALARM Find authenticated court documents without watermarks at docketalarm.com.

DOCKET ALARM

Explore Litigation Insights

Docket Alarm provides insights to develop a more informed litigation strategy and the peace of mind of knowing you're on top of things.

Real-Time Litigation Alerts

Keep your litigation team up-to-date with **real-time alerts** and advanced team management tools built for the enterprise, all while greatly reducing PACER spend.

Our comprehensive service means we can handle Federal, State, and Administrative courts across the country.

Advanced Docket Research

With over 230 million records, Docket Alarm's cloud-native docket research platform finds what other services can't. Coverage includes Federal, State, plus PTAB, TTAB, ITC and NLRB decisions, all in one place.

Identify arguments that have been successful in the past with full text, pinpoint searching. Link to case law cited within any court document via Fastcase.

Analytics At Your Fingertips

Learn what happened the last time a particular judge, opposing counsel or company faced cases similar to yours.

Advanced out-of-the-box PTAB and TTAB analytics are always at your fingertips.

API

Docket Alarm offers a powerful API (application programming interface) to developers that want to integrate case filings into their apps.

LAW FIRMS
Build custom dashboards for your attorneys and clients with live data direct from the court.

Automate many repetitive legal tasks like conflict checks, document management, and marketing.

FINANCIAL INSTITUTIONS
Litigation and bankruptcy checks for companies and debtors.

E-DISCOVERY AND LEGAL VENDORS
Sync your system to PACER to automate legal marketing.